

# Inevitable consequences of ion-neutral damping of intermediate MHD waves in Sun-like stars

Philip G. Judge<sup>\*</sup>

*High Altitude Observatory,  
National Center for Atmospheric Research,  
Boulder CO 80307-3000, USA*

Accepted . Received ; in original form

## ABSTRACT

In the context of the solar atmosphere, we re-examine the role of neutral and ionized species in dissipating the ordered energy of intermediate-mode MHD waves into heat. We solve conservation equations for the hydrodynamics and for hydrogen and helium ionization stages, along closed tubes of magnetic field. First, we examine the evolution of coronal plasma under conditions where coronal heating has abruptly ceased. We find that cool ( $< 10^5$  K) structures are formed lasting for several hours. MHD waves of modest amplitude can heat the plasma through ion-neutral collisions with sufficient energy rates to support the plasma against gravity. Then we examine a calculation starting from a cooler atmosphere. The calculation shows that warm ( $> 10^4$  K long ( $>$  several Mm) tubes of plasma arise by the same mechanism. We speculate on the relevance of these solutions to observed properties of the Sun and similar stars whose atmospheres are permeated with emerging magnetic fields and stirred by convection. Perhaps this elementary process might help explain the presence of “cool loops” in the solar transition region and the production of broad components of transition region lines. The production of ionized hydrogen from such a simple and perhaps inevitable mechanism may be an important step towards finding the more complex mechanisms needed to generate coronae with temperatures in excess of  $10^6$  K, independent of a star’s metallicity.

**Key words:** Sun: corona; Sun: atomic processes; Physical Data and Processes; stars: coronae; Sun: chromosphere; UV radiation: The Sun

## 1 STATEMENT OF THE PROBLEM

This paper re-examines influences of intermediate MHD waves on the solar atmosphere above the stratified chromosphere. Direct observational signatures of such waves with periods of several minutes has been documented for more than a decade (Tomczyk et al. 2007; McIntosh et al. 2011). When account is taken of likely wave amplitudes inferred from measured widths of chromospheric and coronal emission lines at visible (Billings 1966) and UV wavelengths (Cheng et al. 1979; Doschek & Feldman 2000; Brooks & Warren 2016), the energy flux of such waves appears ample to support radiative and other losses from the solar corona. It is well-established that frictional and viscous forces are unable to dissipate these waves quickly enough in highly ionized plasma, unless dynamical processes, such as phase-mixing and resonant absorption, can generate structure on scales far below the typical wavelengths. Some difficulties

with such proposed mechanisms have been highlighted by, for example, Parker (1991); Ofman et al. (1998); Cargill et al. (2016), and the complexity of the problems that these mechanisms entail make this an active research area today.

However, two articles have re-emphasized the role of ion-neutral friction in heating the corona (Zaitsev & Shibasaki 2005; Wójcik et al. 2020). In both studies, the fractions of neutral atoms greatly exceed those expected under conditions of coronal ionization equilibrium. Figure 1 shows ionization fractions computed under optically thin, radiation-free conditions using the HAQS-DIPER package (Judge 2007). In Zaitsev & Shibasaki (2005), the ionization fraction of neutral helium above  $10^6$  K exceeds  $10^{-5}$ , where our calculations indicate values below  $10^{-8}$ . The difference is seen explicitly through their equations (23) and (24), which neglects ionizations from  $\text{He}^+$  to  $\text{He}^{2+}$ . Figure 1 highlights how this affects the coronal fractions of neutral He, the dashed line is equivalent to the calculation of Zaitsev & Shibasaki (2005).

Wójcik et al. (2020) made 2D MHD calculations in

\* E-mail: judge@ucar.edu

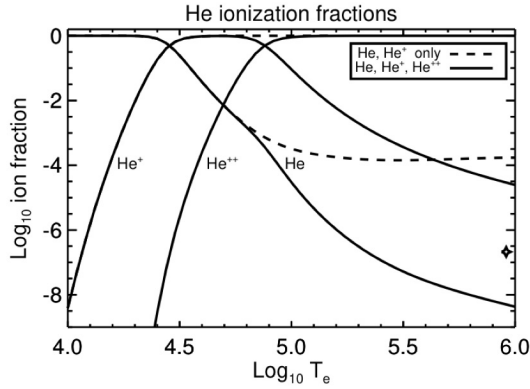


**Figure 1.** Ionization equilibrium calculations for helium, using only He, He<sup>+</sup> (dashed lines) and using all three stages of ionization (solid). Only collisions with electrons have been included. The difference between the dashed and solid lines for neutral helium reveals the erroneously high He neutral populations computed by Zaitsev & Shibasaki (2005). The star symbol shows the ion fraction for neutral hydrogen near 10<sup>6</sup>K.

a two fluid model of the solar atmosphere including ion-neutral collisions. Their calculations show even higher neutral fractions in the corona than were found by Zaitsev & Shibasaki (2005), because no sources or sinks of ionization and recombination by collisions with electrons were treated. Instead the authors including only the advection term in their solutions for number densities.

One dimensional (i.e. field-aligned) hydrodynamical models of the chromosphere and corona have been studied for several decades. Early work includes Oran et al. (1982); Peres & Serio (1984); Mariska (1987); Korevaar & van Leer (1988), and more recent advances including adaptive numerical resolution, first applied by McClymont & Canfield (1983) to the transition region, are summarized by, e.g., Hansteen (1993); Bradshaw & Cargill (2013); Polito et al. (2018). Two- and three- dimensional models (Roussev et al. 2002; Gudiksen et al. 2011; Rempel 2017) including magneto-hydrodynamics, radiative transfer, ion-neutral physics and field-aligned connections to the solar corona have been developed. The latest 3D models required enormous efforts by many people over years. They currently represent the closest numerical work to genuine “simulations” of the solar atmosphere (as opposed to numerical experiments), and represent the state of the art.

Yet, we believe that a class of quasi-stable solutions may have been missed. Litwin & Rosner (1993) concluded from elementary considerations that coronal heating “must be impulsive in onset.” Many papers have provided observational and theoretical evidence for coronal heating that is intermittent in space and time (see reviews by Klimchuk 2006; Parnell & De Moortel 2012; De Moortel & Browning 2015). This result is a consequence of the special conditions needed to generate the necessarily small scales, which arise naturally under local and non-local conditions from intermediate wave resonances and the slower build up of magnetic stresses (Ionson 1978; Parker 1988). Once this heating has occurred, the small structures will evolve rapidly, which will either dampen or enhance the small-scale energy dissipa-

**Table 1.** Logarithmic values of typical physical parameters

Quantity	unit	values		
$T$	K	4.0	5.0	6.0
$n_e$	cm <sup>-3</sup>	10.4	9.4	8.4
$\rho$	g cm <sup>-3</sup>	-13.0	-14.0	-15.0
$B$	G	_____	1.0	_____
$\Omega_i$	rad s <sup>-1</sup>	_____	5.0	_____
$2\pi/\Omega_i$	s	_____	-4.2	_____
$\tau_{ee}$	s	-6.0	-3.5	-1.0
$\tau_{ii}$	s	-4.4	-1.9	0.6
$\tau_{ie}$	s	-2.5	-0.5	1.5
$\tau_{in}^*$	s	-2.9	2.5	4.6
$\tau_{in}$	s	-2.4	3.0	5.1
$\tau_{rec}^a$	s	2.0	3.5	5.0
$\tau_{ion}^b$	s	4.3	-1.3	-1.4
$\tau_{pion}^c$	s	_____	2.0	_____
$\tau_{tion}^d$	s	2.0	-1.3	-1.4
$n_H/(n_H + n_p)$		-0.3	-4.8	-6.5
$L^e$	cm	_____	9.7	_____
$F_R^f$	erg cm <sup>-2</sup> s <sup>-1</sup>	_____	5.4	_____
$F_R/L^g$	erg cm <sup>-3</sup> s <sup>-1</sup>	_____	-4.3	_____
$\tau_{cool}^h$	s	_____	3.3	_____
$L/c_S$	s	3.7	3.2	2.7
$L/c_A$	s	2.7	2.2	1.7
Wave period $P_W^i$	s	_____	2.3, 3.0	_____
Wave freq. $\omega$	rad s <sup>-1</sup>	_____	-1.5, -2.2	_____

Physical properties of the calculations are listed as base 10 logarithms. All quantities refer to a pure hydrogen atmosphere at a constant pressure of  $p = 0.07$  dyne cm<sup>-2</sup>. The quantities  $\tau_{in}$  refer to time scales for collisions on ion  $i$  by neutral  $n$ , and so forth. \*The value is for momentum-changing charge-transfer transitions (eq. A17 of Gilbert et al. 2002), the unsuperscripted value of  $\tau_{in}$  is for elastic collisions (Hunter & Kuriyan 1977). <sup>a</sup>Recombination times for protons colliding with electrons, <sup>b</sup>ionization times for hydrogen atoms colliding with electrons, both estimated using data from Allen (1973). <sup>c</sup>photoionization times, from Ogawa et al. (1995) (for helium, we use Sokół & Bzowski 2014). <sup>d</sup>total ionization times. <sup>e</sup>Loop length, <sup>f</sup>energy flux density needed to support the overlying corona, <sup>g</sup>inferred heating rate, <sup>h</sup>cooling time, <sup>i</sup>the wave period used for intermediate waves.

tion. Thus, if the development of small scales is indeed the pre-requisite for coronal heating, then the heating process inevitably must be intrinsically *dynamic and intermittent*.

Our goal therefore is to examine the dynamics of plasma in tubes of magnetic flux *between the episodes of strong coronal heating*, such as when the resonance condition of Ionson or the “critical angle” condition for Parker’s nano-flares are not met. We build a model containing the fewest ingredients that can transport and deposit energy above the chromosphere. All stars that rotate and convect will have varying emergent magnetic fields (Spruit 2011), and all Sun-like stars in the solar neighborhood of the Galaxy possess hot coronae (Schmitt 1997), and an abundance of ionized atoms. Between episodes of coronal heating, all such stars must experience the effects of ion-neutral collisions on intermediate waves. Thus we re-examine intermediate MHD waves dampened by ion-neutral collisions.

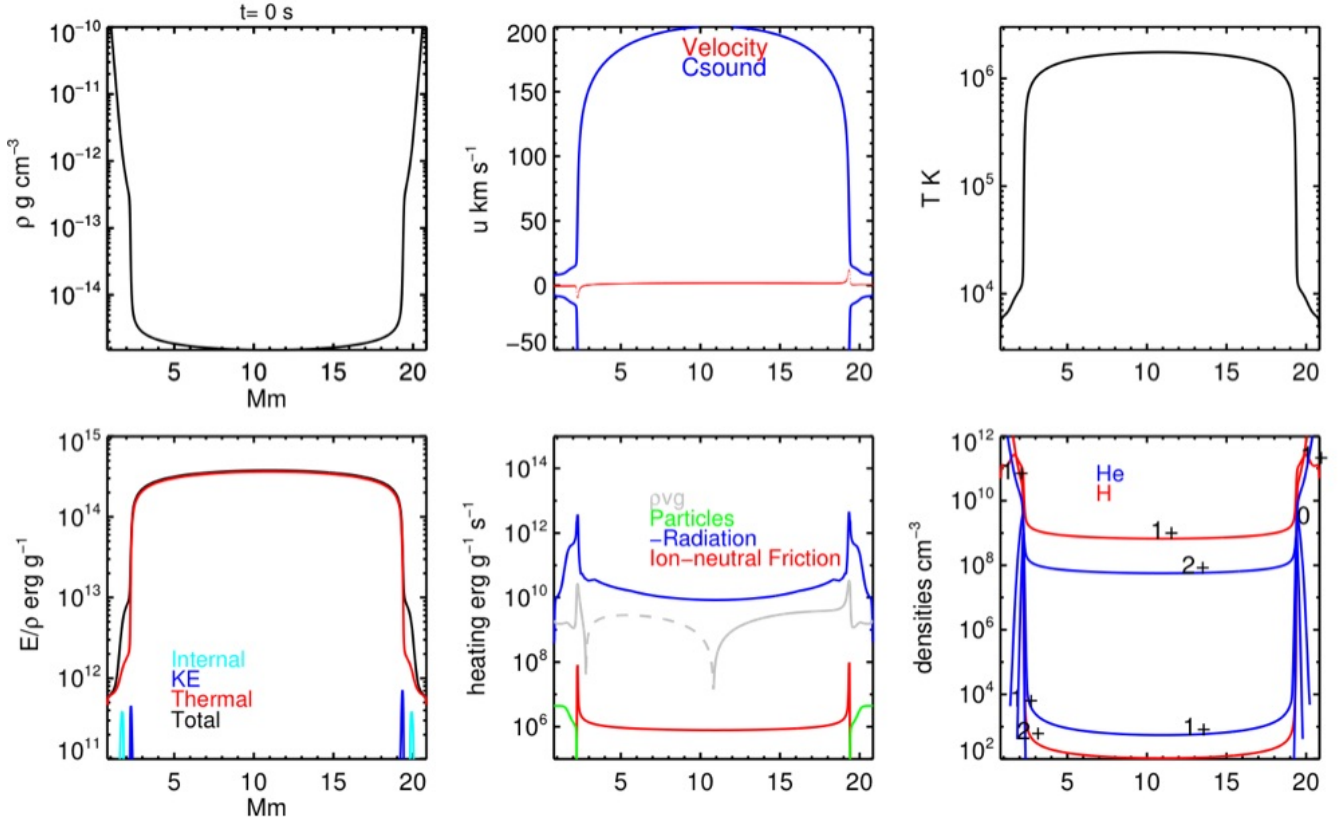


**Figure 2.** Initial state for calculations with  $L = 20$  Mm. The curves labeled “particles” in the bottom middle panel is the heating of neutrals used at the footpoints to support the modeled “chromosphere” at the base. The upper middle panel shows flow speeds spanned by sound speeds in the forward and backward (negative values) directions. Note that the energy densities of the intermediate waves are not plotted. Negative values of are shown as dotted lines in these logarithmically-scaled plots.

## 2 CALCULATIONS

### 2.1 A minimal framework

We perform numerical calculations of a partially-ionized hydrodynamic plasma, solving for the evolution of mass density, momentum and energy along a tube of flux. As is usual, we assume that departures from thermal distribution functions are *small* because of the relatively rapid exchange of energy and momentum between like particles (e.g. [Braginskii 1965](#), see the estimates in [Table 1](#)). We also assume that all particles have the same temperature, although the energy equilibration times between particles of disparate mass can exceed dynamical evolution times ([Table 1](#)). But unless the ion and neutral temperatures exceed electron temperatures by more than factors of 40 or more, only the electron temperature controls collision times for electron-particle collisions. The long ionization and recombination times for a given electron temperature can greatly exceed dynamical times, so therefore we must solve for populations of hydrogen and helium neutral and their ions, writing these collisional terms as source and sink terms in the conservation equations for hydrogen and helium. The solution “vector” evolved in time and space is therefore

$$(\rho, \rho u, E, n_{\text{H}}, n_{\text{H}^+}, n_{\text{H}^-}, n_{\text{He}}, n_{\text{He}^+}, n_{\text{He}^{++}}) \quad (1)$$

where  $\rho$  is the mass density (a sum of particle masses and number densities),  $u$  the fluid velocity,  $E$  the total energy,

and  $n_i$  the various number densities of the constituent ions. The electron density  $n_e$  is the sum of all free electrons from H and He, and then the equation of state is used to determine the temperature  $T$ . Being a 1D calculation, there is no explicit dynamics perpendicular to the magnetic field. Instead, the dynamics is captured implicitly through the heating term in the energy equation (see [equations 6 and 7](#) below). The intermediate waves drive perpendicular macroscopic drifts between ions, electrons and neutral species. The kinetic energy of these drifts is destroyed by random collisions leading to irreversible energy exchange, as is readily understood as the conversion of bulk motion (the different centroids of the distribution functions) into heat (widths of distribution functions).

The interaction of intermediate waves with a partly-ionized plasma depends on various time scales, from collision times between abundant particles (predominantly atoms and ions of H and He, and electrons), periods of gyro-motion of ions, to wave oscillation periods (e.g. [Braginskii 1965](#), section 8). [Table 1](#) lists the parameters most relevant for this study, presented for hydrogen only, for clarity or presentation. Values for time scales for helium impact with other particles were used from [Judge \(2007\)](#) and [Gilbert et al. \(2002\)](#).

**Table 2.** Adopted intermediate wave flux densities

$F_W$ erg cm <sup>-2</sup> s <sup>-1</sup>	Initial $\xi$ km s <sup>-1</sup>	B G
10 <sup>3</sup>	1	10
10 <sup>4</sup>	3	10
10 <sup>5</sup>	10	10

## 2.2 Dissipation of intermediate waves

Consider an intermediate mode with amplitude  $\xi$  cm s<sup>-1</sup> and group velocity  $v_g$  propagating along a magnetic line of force. Again, for clarity we consider here a hydrogen plasma, below we include helium explicitly, and treat radiation losses of trace species using a lookup table. We follow section 3 of [Holzer et al. \(1983\)](#). The flux density of energy carried by the wave motion is

$$F = \rho \xi^2 v_g \text{ erg cm}^{-2} \text{ sec}^{-1}, \quad (2)$$

For the intermediate mode,  $v_g$  equals the Alfvén speed  $c_A = B/\sqrt{4\pi\rho_i}$ .  $\rho_i = n_i m_H$  is the mass density of protons with number density  $n_i$ , or  $c_A = B/\sqrt{4\pi m_H(n_i + n_n)}$  if the ions exchange momentum with ambient neutrals with number density  $n_n$ , on a time scale which is much less than the wave period  $P_W$  (Table 1). This condition is valid below the corona. Within the corona there are so few neutrals that one can set  $n_i \approx n_i + n_n$  so that the plasma inertia throughout the atmosphere can be written using  $m_H(n_i + n_n)$  everywhere.

The ions must be magnetized ( $\Omega_i \tau_{in} \gg 1$ ), in order that the magnetic wave motions drag ions through neutral gas with significant drift speeds. Here  $\Omega_i$  is the ion gyro frequency ([Braginskii 1965](#)):

$$\Omega_i = \frac{eB}{m_i c} = 0.96 \cdot 10^4 B \quad (3)$$

for protons. In typical models with magnetic fields concentrated in kG fields in the photosphere, extending to 1-10 G in the corona, the protons are strongly magnetized across the chromosphere and corona (see Table 1).

The volumetric fluid heating rate for an ion-neutral drift speed  $\bar{u}$  is (see page 812 of [Holzer et al. 1983](#)):

$$\dot{E}_v \approx \frac{1}{\tau_{in}} \rho_i \bar{u}^2. \text{ erg cm}^{-3} \text{ sec}^{-1}, \quad (4)$$

At low wave frequencies  $\omega$  ( $\omega \tau_{in} \ll 1$ ), collisions dominate the dynamics of ions and neutrals, the resulting diffusion leads to a small drift speed  $u$ :

$$\begin{aligned} \bar{u} &\approx \omega \tau_{in} \cdot \xi \text{ cm sec}^{-1}, \\ &\ll \xi \end{aligned} \quad (5)$$

where  $\xi$  is the wave amplitude in cm sec<sup>-1</sup>. In the opposite limit where  $\omega \tau_{in} \gg 1$ , the drift speed  $\bar{u} \approx \xi$ . Then, for both cases we can write

$$\dot{E}_v \approx \frac{(\omega \tau_{in})^2}{1 + (\omega \tau_{in})^2} \frac{1}{\tau_{in}} \rho_i \xi^2 \text{ erg cm}^{-3} \text{ sec}^{-1}, \quad (6)$$

The heating per unit mass is

$$\dot{E}_m \approx \frac{\dot{E}_v}{m_H(n_i + n_n)} \quad (7)$$

$$\approx 0.9 \cdot \sqrt{T} n_{<} \xi^2 \text{ erg g}^{-1} \text{ sec}^{-1}, \quad (8)$$

in erg g<sup>-1</sup>sec<sup>-1</sup>, where  $n_{<}$  is the smaller of  $n_i$  and  $n_n$ , and  $\xi_5 = 10^5 \xi$ .  $\xi_5$  is the drift speed in km s<sup>-1</sup>. Here we have used the elastic collision rate between protons and H atoms,  $\tau_{in}$ .

Since the drift speed  $u$  also constitutes an electric current, the frictional dissipation can also be written in terms of an electric current and a conductivity, which for motions across the field is the perpendicular conductivity (page 281 of [Braginskii 1965](#)). Under weakly ionized or cold plasma conditions, the latter can be treated using ‘‘Cowling’s conductivity’’ ([Cowling 1956](#)). The conductivity approach has been implemented in modern 3D MHD codes.

Below we will study calculations with fixed input energy flux densities of intermediate waves which, in the initial state, produce rms wave amplitudes of 1, 3 and 10 km s<sup>-1</sup> within the initially hot coronal plasma (Table 2), all of which are modest values compared with observations (e.g. [McIntosh et al. 2011](#)). These initial amplitudes change in time as the densities evolve during the calculations. We made calculations with wave periods  $P_W$  of 180 and 1000 seconds for reasons given below. We also make the assumption that damping is weak and use a constant wave flux along each tube. In section 3.2 we will find that the damping lengths

$$L \approx c_A \tau_{in} \text{ cm} \quad (9)$$

([Holzer et al. 1983](#), eq. 16) exceed the lengths of the tubes.

## 2.3 Numerical Method

We solve equations for the conservation of mass, momentum, energy and the number densities listed in the vector (1), for a single fluid. The vector components are solved as a function of time and distance along a closed flux tube. The geometry is a simple arc of a circle which intersects the lower atmosphere at a given height near the photosphere, with no geometric expansion. Three types of calculations were made, the arc center being at the footpoint height and in a vertical plane, some calculations with a modified gravity accounting for an arc in a plane tilted to the vertical, and calculations where the center of the circle defining the arc is displaced a few Mm below and above the footpoints. These geometries serve to test how the gravity vector affects coupling between the chromosphere (< 2Mm height) and the higher regions.

All variables at each (deep) footpoint were held fixed at the initial state, where  $\log_{10} \rho \approx -9.22$  g cm<sup>-3</sup> (cf. the values much higher up in the atmosphere in Table 1). While the model is almost symmetric around the mid-point, the boundaries were set to values differing by 10% in density to introduce a little asymmetry in the dynamics, since in the real Sun the two boundaries are different. At these densities, which lie 700 km above the continuum photosphere of traditional models, they are about 9 pressure scale heights below the initial transition region. The conservation equations for for populations of H atoms, protons, helium atoms, He<sup>+</sup> and He<sup>2+</sup> ions include the advection and ionization and recombination terms (see the Appendix of [Judge et al. 2012](#)). The scheme can be seen as a simplified version of a multi-fluid calculation in which the ion-neutral collisions induced by wave motions perpendicular to the general magnetic field direction serve to heat the fluid.

The force balance includes the pressure gradient and gravity vector projected along the direction of the flux tube,

$g(s)$ . With the assumption of weak dissipation, the momentum transfer to the fluid from the waves, is negligible compared with the gravity and pressure gradient terms (Hartmann & MacGregor 1980, section 3(b)). The energy balance includes the explicit heating terms of equation (6), heating due to EUV radiation from the ambient corona, and explicit radiation losses computed as a function of time for H and He, and as a lookup table for the trace species such as C, N, O etc. (Judge et al. 2012). The energy equation is

$$\frac{\partial}{\partial t} E + \frac{\partial}{\partial s} u(E + p) = \dot{E}_V + \mathcal{H}_{\text{EUV}} + \mathcal{H}_{\text{CHR}} - C_R \quad (10)$$

$$- \rho g(s)u + \frac{\partial}{\partial s} \left( \kappa T^{5/2} \frac{\partial T}{\partial s} \right) \quad (11)$$

where

$$E = \sum_i \frac{n_i k T}{\gamma - 1} + \frac{1}{2} \rho u^2 + U \quad (12)$$

is the total energy per unit volume, the sum is over all particles, and  $\gamma = 3/2$  because internal energy is explicit in  $U$ .  $\kappa = 10^{-6}$  is the Spitzer coefficient of heat conduction,  $\mathcal{H}_{\text{CHR}}$  is a small *ad-hoc* heating term to maintain the chromosphere against strong radiation losses near the footpoints (Hansteen 1993). We used  $\mathcal{H}_{\text{CHR}} = 10^{-17}$  erg particle $^{-1}$  s $^{-1}$ . The curves labeled “particles” in the following figures show this term.  $C_R$  is the (positive definite) radiative loss term, and  $U$  is the latent heat of ionization computed directly from the ionization potentials and number densities of ions, including a correction for the fact that hydrogen is ionized by the external source of radiation formed in the photosphere, in the Balmer continuum.

We use a first-order Lax-Friedrichs explicit integrator in time (Tóth & Odstrčil 1996). This scheme avoids use of characteristic variables. The equations are written and solved in conservative form, but an operator splitting technique is adopted to solve for the field-aligned electron heat conduction (Judge et al. 2012). We used uniform grids with spacings of about 10 km, to try to resolve the transition region. There is of course implicit dissipation owing to the numerical scheme, causing smoothing in space close to steep gradients (shocks and the steep transition region). We found that the extension to second-order scheme using total variation diminishing methods (Tóth & Odstrčil 1996), while less dissipative, was far less robust. The conservative formulation guarantees that only smoothing occurs, and the final equilibrium states contain no steep gradients. Our main conclusions therefore are not strongly dependent on numerical diffusion.

We made calculations for tube lengths  $L$  of 10, 20, 30, and 40 Mm, using wave periods  $P_W$  of 180 and 1000 seconds. We used a field strength of  $B = 10$  G and wave flux densities  $F_W$  of  $10^3$ ,  $10^4$  and  $10^5$  erg cm $^{-2}$  sec $^{-1}$ . With these conditions the largest wave amplitudes  $\xi$  at the start of each calculation were 1, 3 and 10 km s $^{-1}$  respectively. The calculations made are summarized Table 3.

## 2.4 Relaxation following coronal heating

The first calculations we made were started from a model close to force and energy balance with steady heating rates of  $2 \cdot 10^{-12}$  and  $2 \cdot 10^{-14}$  erg particle $^{-1}$  s $^{-1}$  for protons

and neutrals respectively, run until almost static (all velocities well below all sound speeds). The goal was merely to begin from a physically realistic coronal state. Anderson & Athay (1989) found that heating rates  $2 \cdot 10^{-13}$  and  $2 \cdot 10^{-14}$  erg particle $^{-1}$  s $^{-1}$  – corresponding to  $10^{11}$  and  $10^{10}$  erg g $^{-1}$  s $^{-1}$  – were required to support the average quiet solar corona and chromosphere respectively. Our initial state (calculation “initial” in Table 3) is representative of a more aggressively heated corona, with coronal pressures of between 0.17 and 0.6 dyne cm $^{-2}$ . In contrast, the quiet Sun’s coronal pressure is about 0.08 dyne cm $^{-2}$ . The thermodynamic structure is shown in Figure 2.

From this initial state, the steady heating rates of protons and neutral particles that led to the formation of the  $10^6$  K corona were set to zero, and the calculation allowed to relax, including only the heating through the  $\dot{E}_V$ ,  $\mathcal{H}_{\text{CHR}}$ , and for half of the cases the  $\mathcal{H}_{\text{EUV}}$  terms. In making these calculations we attempt to model the situation where intermediate waves persist, but the special conditions leading to coronal heating do not occur. Figures 3 and 4 show intermediate and final calculations for a  $L = 20$  Mm calculation driven by waves of  $P_W = 180$  second period and wave flux  $F_W$  of  $10^4$  erg cm $^{-2}$  s $^{-1}$ , which is calculation 20 in Table 3. The behavior seen is typical of others listed in the Table and marked as “EQ”, signaling a near-equilibrium final state. These calculations continue to evolve very slowly, but the important result here is that, compared with dynamical time scales, these are *extremely long-lived*.

During the first hour of evolution (Figure 3), the pressure gradient supporting the initial state is reduced as the tube cools, the dynamics forming a simple downflow to the footpoints until the upper chromosphere is reached, where a shock is formed. This collapse towards a chromospheric state is as many other calculations have found (e.g. Field 1965; Cally & Robb 1991). But unlike earlier work, the interplay between ion-neutral heating, thermal evolution and the evolving times of recombination and ionization reveals new classes of solutions governed by these non-linear interactions. Some of these non-linearities are revealed by comparing calculations with and without EUV photo-ionization (Table 3 and Figure 5). For example, an increase in photo-ionization (itself a source of heating) decreases neutral hydrogen densities, which in some cases leads to smaller peak temperatures (calculations 11,12), and vice-versa (calculations 1,2 or 7,8).

Figure 5 attempts to show graphically the main results and trends listed in Table 3. All calculations shown began with the coronal initial state. The  $L = 20$  Mm parameters at the tube top are listed in the top right of each panel. Larger circles show larger lengths  $L$ , and the colors represent the values of  $F_W$ . The difference between the EUV and no-EUV ionization cases are highlighted by the straight lines connecting the “x-ed” (EUV) and open circles. The cluster of red lines near  $\log T = 4.7$  shows those calculations with large  $F_W$  which move up and to the left (near  $\log T = 4.5$ ) when EUV radiation is included. EUV radiation in these cases tends to increase the final density and (perversely) the ratio of neutral to ionized hydrogen  $n_{\text{H}}/n_{\text{p}}$ . The yellow lines ( $\log F_W = 4$ ) show a similar result at lower temperatures for shorter tubes. Yet radically different behavior is seen for the low  $F_W = 3$ ,  $L = 10$  Mm cases. (Longer tubes underwent a catastrophic collapse for  $F_W = 3$ ). These two

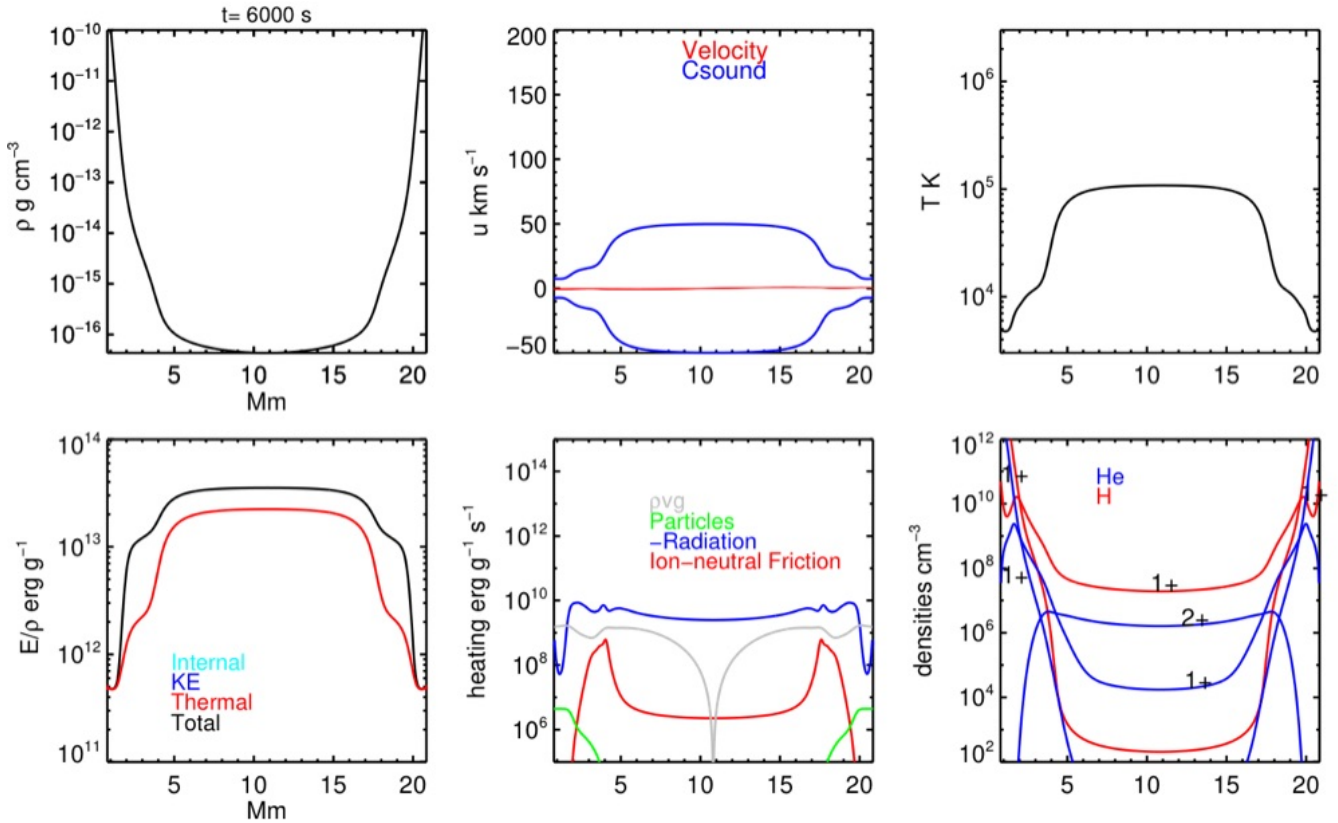


**Figure 3.** State of calculation 20 after  $t = 100$  minutes. Notice that the ratio of neutral hydrogen to protons has increased to  $\approx 10^{-5}$  following advection and recombination. This leads to the significant heating rate shown in red in the middle-lower panel of between  $10^8$  and  $10^{10}$   $\text{erg g}^{-1} \text{s}^{-1}$ , between 4 and 17 Mm along the bundle. In contrast, the initial state (Figure 2) has a ratio of neutral to ionized hydrogen of  $10^6$  with no significant ion-neutral heating.

results highlight again the non-linear sensitivity of the dynamical evolution to the process of wave-driven ion-neutral collisions. The two different behaviors seem to indicate the presence of bifurcations towards dynamical attractors.

For each calculation with a wave flux density  $F_W$  in excess of  $10^4$   $\text{erg cm}^{-2} \text{s}^{-1}$ , a steady state was reached after a relaxation time of order  $\tau_C$  ( $\approx 2000$  seconds, Table 1) or longer, depending on the tube length  $L$ . It should be noted that the pressures at the cool tube tops are always much less than the initial starting pressures by between 2 and 5 orders of magnitude. On the other hand these structures have lengths orders of magnitude larger than the temperature scale height of the classical transition region ( $\approx 10$ – $100$  km). This difference suggests that these structures might be observable (see section 2.6). An example of catastrophic cooling of a heated coronal tube, calculation 13, is shown in Figure 6. This then represents another potential “attractor” state for these non-linear calculations.

Many of the calculations presented in Figure 5 have ratios of  $n_H/n_p > 10^{-4}$ . Here then is the (unanticipated) reason why the mechanism can support long-lived, many Mm-long tubes of cool plasma, almost in hydrostatic equilibrium with the reduced (field-aligned) solar gravity. The result is a surprise given the long-known tendency for cool loops to collapse thermally, given ad-hoc heating mechanisms (e.g. Field 1965; Mariska 1992, and the many references in the latter).

In one calculation we repeated calculation 13 (the case of catastrophic collapse) with a gravity half that of the Sun, i.e. for a tube inclined at  $60^\circ$  to the vertical. This calculation (number 31) stabilized to a state somewhat similar to the equilibrium states for  $L = 40$  Mm.

Lastly, calculations with  $P_W = 1000$  seconds show essentially the same results. The period of these waves determines the factor

$$\frac{(\omega\tau_{in})^2}{1 + (\omega\tau_{in})^2}$$

in equation (6). This factor has little effect on the calculations, for at heights originally occupied by the coronal ( $10^6$  K) plasma, this factor is one throughout the calculation. Instead, a larger consideration concerns the average transverse distance  $\delta$  travelled by the ionized component of the fluid over  $P_W$ . Under collisionless conditions,

$$\delta = \frac{P_W}{2\pi} \xi \quad (13)$$

which for  $\xi = 10$   $\text{km s}^{-1}$  is 286, 1590 km for  $P_W = 180, 1000$  respectively. Evidence for sinusoidal excursions of a few Mm owing to intermediate waves has been reported (McIntosh et al. 2011). This means that the ions potentially will be swept over neutrals existing between neighboring magnetic flux tubes, with different (field-aligned) thermal histories.

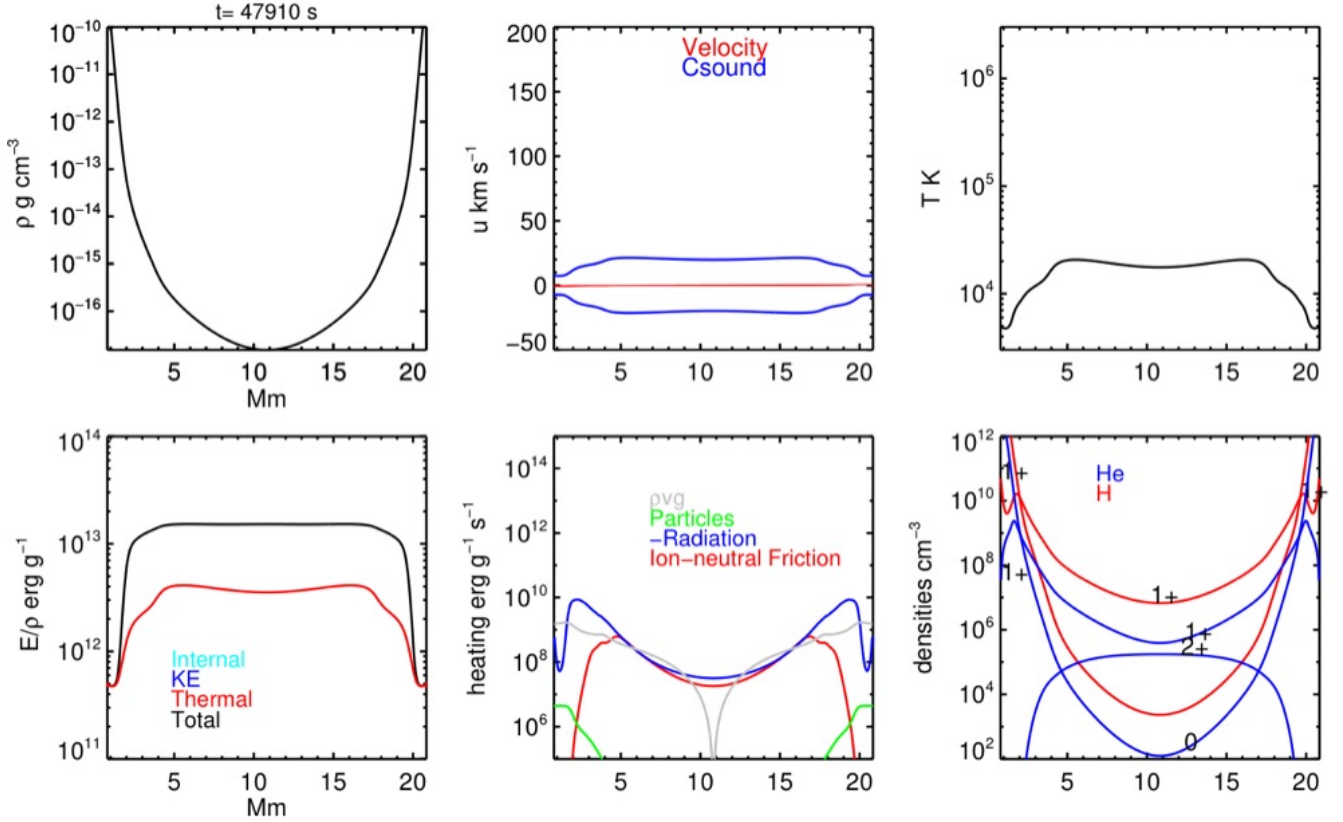


Figure 4. State of calculation 20 after  $t=800$  minutes.

In summary, several trends are evident in the table and Figure 5:

- (i) The primary determinant of equilibrium or collapse is the *wave energy flux density*  $F_W$ ;
- (ii) The second factor determining the fate of the calculation is the tube length,  $L$ . No EQ solution was found for  $L > 20$  Mm when  $F_W = 10^3 \text{ erg cm}^{-2} \text{ s}^{-1}$ ;
- (iii) The third factor is the presence of EUV ionizing radiation, as a source of ions, a reducer of neutrals, and as a source of heat (kinetic energy of freed electrons);
- (iv) EQ outcomes can occur for long wave periods  $P_W$ ;
- (v) For a given wave flux density  $F_W$  both the temperatures and pressures at the tube apex are higher for longer tubes;
- (vi) Changing the plane of the tube relative to the local vertical produces more stable solutions (calculation 31 shown in Figure 7). In this calculation just one half of the pressure gradient was needed to make the solution approach a stable equilibrium.

Frictional heating increases as the fluid cools, atoms slowly recombine, and ion-neutral collisions increase, leading to an increase in heating. In many realizations, this leads to dynamical stability. Wave damping lengths are found *post-facto* to exceed the lengths of the tubes considered (section 3.2).

## 2.5 Evolution starting from a cool atmosphere

The solutions for tubes where heating sufficient to support a corona has ceased are of interest concerning the physical connection of the observed chromosphere and corona (e.g. Mariska 1992; Judge & Centeno 2008). However, there is more at stake than such a specific problem in solar physics. Here we address the question: *starting from a very cool atmosphere with very little heating, can this mechanism generate real temperature reversals in the atmosphere?*

To provide an answer, it is sufficient to demonstrate that this can occur for just one calculation. Ideally we would start from an atmosphere in radiative equilibrium, but such models extend only to about 0.7 Mm above the continuum photosphere, at a continuum optical depth of  $10^{-5}$ . The radiative equilibrium atmosphere is not a good starting point from which to evolve the atmosphere of a star with convection anyway, simply because acoustic waves generated by photospheric motions create relatively hotter plasma heated intermittently to above 4000 K (Carlsson & Stein 1995).

Therefore we start with the atmosphere obtained at the end of calculation 3, with a maximum tube temperature of 4080 K. We ran cases with  $P_W = 180$  seconds and  $F_W 10^4$  and  $10^5 \text{ erg cm}^{-2} \text{ s}^{-1}$ . The results are listed as numbers 32 and 33 respectively. The results are clear, *hot ( $10^5 \text{ K}$ ) plasma is readily generated by a moderate flux density of intermediate waves, starting with plasma at temperatures below 5000K*. Given a very weakly ionized initial atmosphere (calculation 3 has  $n_H/n_P > 200$ ), perhaps from acoustic shock heating of the chromosphere or even meteoric impact,

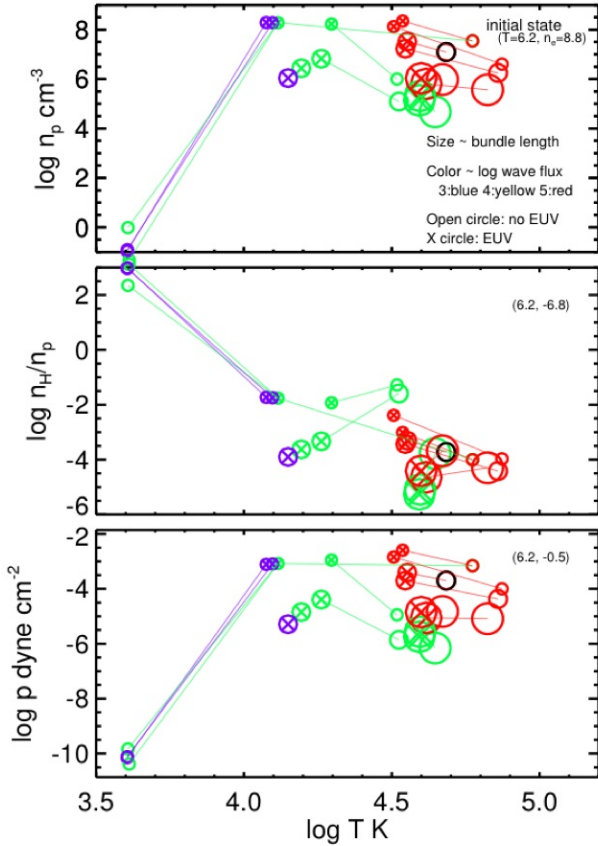


**Figure 5.** Scatter plots are shown using the numbers in Table 3, only for those calculations marked “EQ”. The size of circles indicates the length  $L$  of the bundle for each calculation. The colors represent the amplitude  $\xi$ , blue = 0.6, yellow = 3, red = 10 km s<sup>-1</sup>. The values are for the geometric mid-point (i.e. highest point) of each bundle. The lines plotted connect points where calculations were made with and then without EUV photoionization and heating. Calculation 20 is marked in black.

this mechanism is capable of generating an ionization fraction close to one with large ( $> 10^7$  particles cm<sup>-3</sup>) several Mm above the chromosphere. Thus, *the mere presence of intermediate waves generated by convection suffices to produce a high density, ionized and therefore highly conducting atmosphere*. In this sense this very simple, inevitable mechanism may be an important part of the process leading to stellar coronae, in general.

## 2.6 Observability

From our calculations we can readily find the brightnesses of emission lines between two atomic levels labeled  $j$  and  $i$ . Under optically thin conditions the critical quantity is the emission coefficient integrated over frequency  $\epsilon_{ji}$ :

$$\epsilon_{ji} = \frac{h\nu_{ji}}{4\pi} n_j A_{j \rightarrow i}. \quad (14)$$

$\epsilon_{ji}$  is the frequency-integrated coefficient for total isotropic emission into  $4\pi$  steradians, ignoring stimulated emission, in units of erg cm<sup>-3</sup> sr<sup>-1</sup> s<sup>-1</sup>,  $h$  is Planck’s constant, the line center frequency is  $\nu_{ji}$ ,  $n_j$  the population density of upper level  $j$  and  $A_{j \rightarrow i}$  is the Einstein A-coefficient. Figure 8 shows emission coefficients for the resonance lines of helium along calculation 22, chosen as a calculation with a high pressure at the tube top, and thus it has some of the largest computed coefficients  $\epsilon_{ji}$ . The latter were computed ignoring contributions to line emission from recombination from He<sup>+</sup>. This assumption leads to lower limits on emission which suffices for our purposes. The emergent intensities are

$$I_\nu = \int_S ds \epsilon_{ji} \phi_\nu \quad (15)$$

erg cm<sup>-2</sup> s<sup>-1</sup> sr<sup>-1</sup> Hz<sup>-1</sup>, where  $ds$  is an integration along the LOS  $S$ .  $\phi_\nu d\nu$  is the line profile function, specifying the emission between frequency  $\nu$  and  $\nu + d\nu$  and normalized to an integral over  $\nu$  of 1. To compute  $\phi_\nu$  we added in quadrature the rms thermal and wave amplitudes  $\xi$ , which, as noted above, evolve along with the calculations.

To evaluate the emergent intensity we have a problem in that the line of sight intersects the tube, represented by a line, at a single point of measure zero. So, we must estimate essentially the thickness of the tubes envisaged, which has nothing to do with the 1D calculation, but depends on unknown properties of the original tube of plasma heated to coronal temperatures that has suddenly received no heat. This is beyond current theoretical knowledge, indeed it would require us to have solved the 70+ year-old “coronal heating problem”. This means we must turn to observations and look for consequences which might be refuted in future. The highest resolution coronal images reveal some tubes that appear to be close to a few hundred km (Williams et al. 2020). To be on the conservative side, we adopt a path segment  $ds = 100$  km ( $\equiv 10^7$  cm).

Figures 8 and 9 show emission coefficients and profiles of helium lines during the initial relaxation of the atmosphere from a coronal state, for calculation 22 (table 3). These profiles show the initial dynamic relaxation followed by a slow approach to a near-equilibrium state with a far lower brightness, no Doppler shifts, and broad profiles.

Typical intensities observed in the quiet Sun are 540 and 850 erg cm<sup>-2</sup> s<sup>-1</sup> sr<sup>-1</sup> for the 584 and 304 Å lines of He and He<sup>+</sup> respectively (Pietarila & Judge 2004). So, using  $ds = 10^7$  cm, we find that

$$10^7 \epsilon_{ji} \gtrsim 60,$$

or  $\log \epsilon_{ji} \gtrsim -5.2$  is needed if the mechanisms discussed here are to contribute 10% to the observed level of line emission from a coronal volume. The dashed line of Figure 8 shows this critical value. Note that the value of  $ds = 100$  km for the integration path (equation 15) corresponds to 0.1 Mm on the plot, which is considerably wider than the narrow peaks close to  $t = 0$  s. During the first minute or so, the computed emission may indeed contribute significant emission during the initial dynamic phase. This period of line emission occurs through the work done by gravity on coronal plasma as it collapses down to the chromosphere, compressing the cool plasma and leading to line emission. However, these bright phases occur only along about 0.1-0.2 Mm of the tube length, so would appear as point sources in current



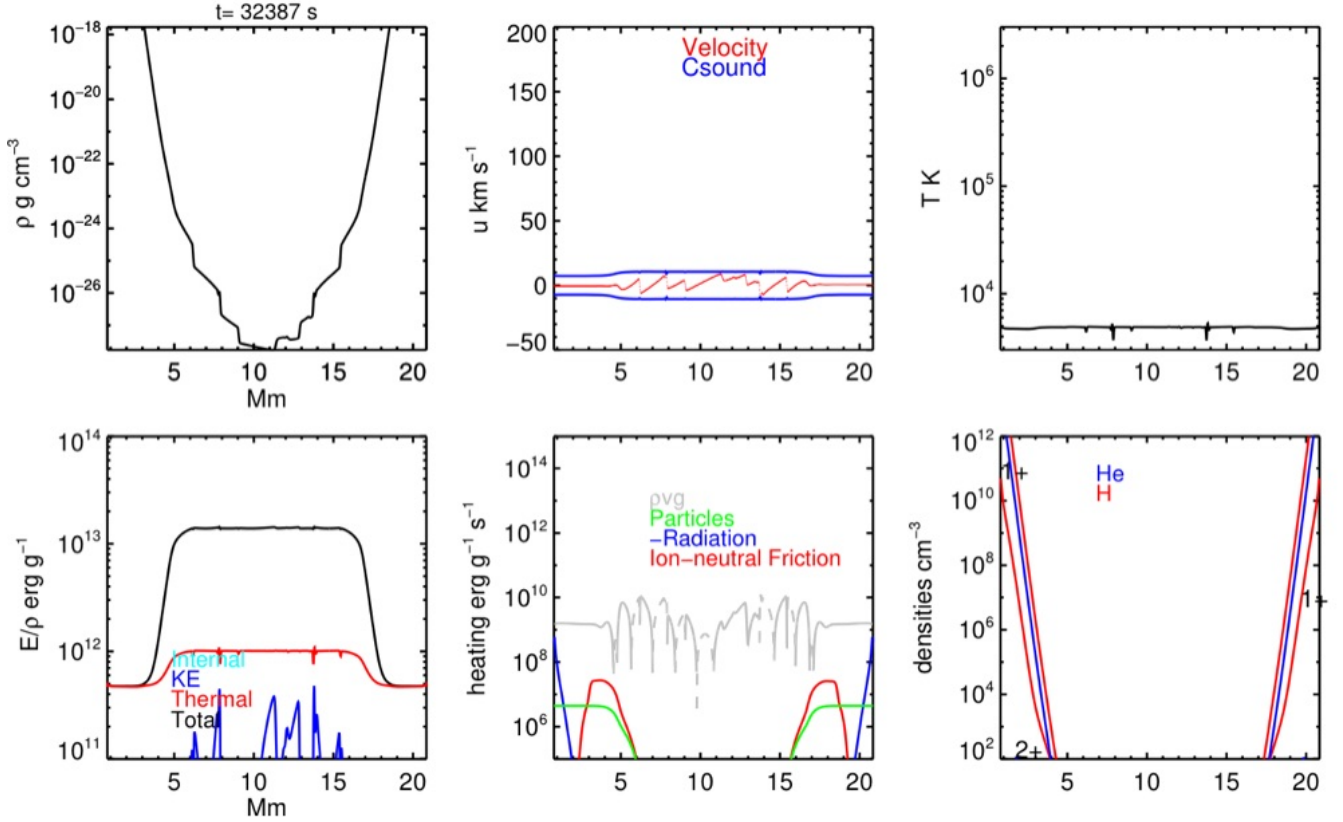


**Figure 6.** State of calculation 13 after  $t=396$  minutes. The fluid calculation has collapsed to a state where mean free paths exceed the size of the system because of the catastrophic loss of support for the atmosphere by insufficient ion-neutral heating. **This implies that a “collisionless” approximation to the transport problem is more appropriate (see text).**

observations. Nevertheless, it appears that the conversion of gravitational energy to radiation through compressive heating may contribute to some observable aspects of emission from lines at transition region temperatures.

At all times beyond a few sound crossing times (1000 seconds or longer), the heating is dominated by ion-neutral collisions. However, the small computed emission coefficients at such times would require path lengths  $ds$  between 1 and 10 Mm to approach the mean observed intensities of the resonance lines of helium.

Figure 9 shows that line profiles after the dynamic phase, i.e. those dominated by the heating by intermediate waves and ion neutral collisions, become broad with widths of tens of  $\text{km s}^{-1}$ . Such widths might conceivably contribute to broad, weak emission seen in many profiles of transition-region emission lines in the Sun and stars, providing perhaps an additional explanation for the existence of such broad components (e.g. Wood et al. 1997; Peter 2006).

Lastly, unless integration paths greatly exceed the assumed value of 100 km, we can surmise that the two heating processes – dynamic compression driven by gravitational collapse, and ion-neutral heating – probably cannot account for the much brighter and long “cool loops” proposed as a solution to a long-standing problem of heating the lower transition region (Cally & Robb 1991; Judge & Centeno 2008; Hansteen et al. 2014).

### 3 DISCUSSION

#### 3.1 Main results

We have identified long-lived, physically extended structures with temperatures between 4000 and  $10^5$  K. They are characterized by having higher fractions of neutral particles than the  $10^6$  K corona by about 3 orders of magnitude. They arise when previously heated coronal tubes of plasma and magnetic flux are no longer aggressively heated to coronal temperatures. These structures should exist when intermediate MHD waves generated by flux emergence and convection drag ions across neutrals which have formed after recombination accompanies plasma cooling. Thus, these structures seem to be inevitable in rotating, convecting stars, which appear to satisfy a sufficient condition for variable magnetic fields to emerge from the stellar surface (Spruit 2011).

There is abundant observational evidence that heating of plasma to coronal temperatures is intermittent in time (see for example Hudson 1991; Kopp & Poletto 1993; Parnell & De Moortel 2012). Further, most theories of coronal heating require special conditions in time and space in order to dump mechanical energy as heat into the corona (e.g. Parker 1994). These special conditions (critical twist, wave resonances, formation of current sheets, magnetic reconnection) all influence the magnetized plasma in a fashion that the heating becomes highly time-dependent. Thus, if the coronal plasma suffers a lack of heating for a cooling time or

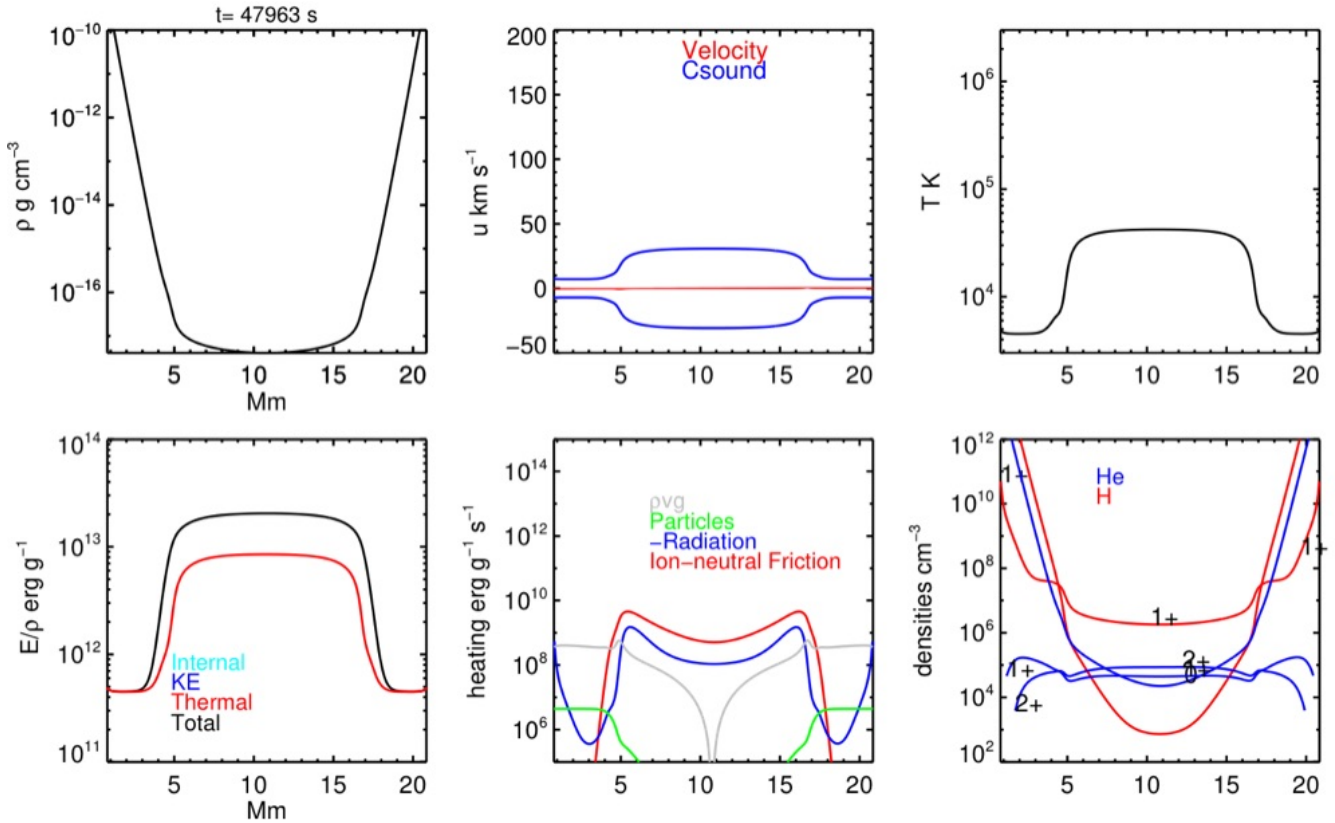


**Figure 7.** State of calculation 31 after  $t=800$  minutes, a calculation identical to the collapsed case (Figure 6) but using a gravity half that of the Sun in the radial direction, for a bundle lying in a plane inclined at  $60^\circ$  to the vertical.

longer, then we must expect these novel structures to exist. Further, we have found that, starting from a very cool atmosphere, reasonable conditions can lead to plasma in long tubes with temperatures exceeding  $10^5$  K.

These new solutions were unexpected by the author, as it is well known that “cool loop” solutions are thermally and hence dynamically unstable (Mariska 1992, see Figure 6 for an example). The significant ion-neutral heating that occurs just above the stratified chromosphere, along with the reduction in the field-aligned component of gravity can maintain a long-lived, quasi-stable structure. The solutions are not strictly in equilibrium, because all solutions have residual flows and waves resulting from the non-linear interactions between heating and the evolving plasma densities. But pressure gradients are almost balanced with the reduced field-aligned component of gravity

Such stable solutions now seem inevitable in most convecting, rotating stars, requiring only:

- (i) The presence of magnetic fields emerging through the photosphere and generated by dynamo action,
- (ii) The presence of perturbations of intermediate waves by convection and/or global modes of oscillation, propagating along these magnetic fields, with
- (iii) wave amplitudes and periods compatible with solar observations,
- (iv) inclusion of frictional heating between protons and hydrogen atoms.

These conditions appear to be *sufficient* to create a minimum level of heating in the outer atmospheres of such stars. Thus *any star with magnetism emerging into the atmosphere, perturbed by convective motions, must possess a cool corona*. This includes low-metallicity stars, because the heating depends only on the presence of hydrogen and helium. It is in the dependence of cooling upon elements other than H and He that such stars will differ. Therefore we expect that these stars will have a different thermal structure from these solar calculations, all other things being equal, as the energy balance is one between local heating and radiative losses from different amounts of trace species.

Returning to solar physics, a robust feature of these simple 1D models is ion-neutral heating that develops throughout the lengths of these flux tubes. We find that the dissipation of magnetic energy here can be  $\gtrsim 10^8$  erg  $g^{-1} s^{-1}$ . It seems possible that, especially above the solar limb, deep EUV observations might be compared with these model predictions, along the lines of recent work by Hahn & Savin (2014), who found energy dissipation within hot coronal tubes occurring over the upper 80% of the loops they observed. Even the absence of predicted features (Figure 9) in deep exposures would put constraints on the nature of intermittency in coronal heating (e.g. Litwin & Rosner 1993). These calculations may have relevance to stellar observations as well as solar, where symmetric, broad components are seen at the base of some transition region lines, usually

explained as explosive events (e.g. Wood et al. 1997; Peter 2000, 2006) .

### 3.2 Limitations

In adopting a single-fluid approximation we implicitly assume that all particles collide between different species at much faster rates than dynamical time scales, exchanging momentum and energy faster than external forces can separate them. The longest time scales for collisions involve ions and neutrals. Thus when  $\tau_{\text{in}}$  exceeds dynamical time scales our approximation will fail. Crudely, taking  $L \approx 10$  Mm and comparing  $\tau_{\text{in}}$  with  $\tau_{\text{S}}$  we find that  $n_{\text{H}} > 3 \cdot 10^5$  atoms  $\text{cm}^{-3}$ . Some of our EQ calculations dip below this limit (Figure 5) but the majority lie above it. This value of  $n_{\text{H}}$  is however a lower estimate when structures, such as shocks, exist on length scales below 1 Mm. In a multi-component plasma, the thermal force (e.g. Braginskii 1965) can lead to a positive force along a temperature gradient akin to a negative heat flux under the effects of heat conduction. While potentially important in regions of steep temperature gradients, it is likely to be small when solutions evolve well below coronal temperatures.

Mean free paths (MFPs) of particles are  $1/n\sigma$ , with  $n$  the number density and  $\sigma$  a collision cross section with similar particles. MFPs for collisions between charged identical particles electrons are smaller than for gas-kinetic (neutral-neutral) MFPs. The ion-neutral and neutral-neutral MFPs are on the order of  $10^{14}/n$  cm. We have made calculations using tubes of length  $L \approx 20$  Mm, so that, for neutrals exhibiting linear motion, we would need  $n_{\text{H}} > 10^5$   $\text{cm}^{-3}$  for the system to be collisional. For protons which exhibit gyro motion, we would require  $n_{\text{p}} > 3 \cdot 10^4$   $\text{cm}^{-3}$ . Even in the “collisionless” limit, modified “collisionless MHD equations” can be derived. For example, collisionless MHD models are applied to Earth’s magnetosphere where the MFP is about a light year (Lyon et al. 2004). Such modifications are not important for the major conclusions of the present work.

More importantly is the need to have many particles in each computational cell, in order that the appropriate averages are meaningful. In our calculations we typically use a cell of at least 10 km. In this case the averages (density, momentum, energy density) are well-defined when  $n > 10^{-4}$  particles  $\text{cm}^{-3}$ . The end states of the catastrophic collapse violate this condition (Figure 6).

The geometry is entirely 1-dimensional, taking no account of the expansion of the tubes of flux from the low chromosphere and into the corona. The expansion leads to an upward magnetic pressure gradient within a tube. But when  $B \gtrsim 1$  G this expansion takes place almost entirely within chromosphere, because it spans some 9 pressure scale heights. Our goal is to study how ion-neutral collisions might lead to effects initially within the (initially) *far more extended corona*. The physics of the chromosphere is certainly important, setting a lower boundary condition for plasma evolution. Our model simply provides a “chromosphere” as a stratified layer with small wave speeds. It serves as a reservoir of mass which can be supplied along flux tubes.

Finally, the assumption of weak wave damping might fail. But for all calculations made here the damping length exceeded 200 Mm in the final state. The flux of intermediate waves is almost undamped.

### 3.3 Future thoughts

This series of calculations was in part prompted by remarkable data from the more extended corona, in which the He I 1083 nm line has been observed to be brighter than predicted, even with recently updated atomic calculations (Del Zanna et al. 2020). With Prof. J. R. Kuhn, the author is investigating ion-neutral and ion-dust-neutral dynamics in the inner heliosphere, following observational work obtained during total solar eclipses for more than two decades (Kuhn et al. 1996; Mann & Kuhn 1998; Kuhn et al. 2007; Moise et al. 2010; Habbal et al. 2018). These are fundamental processes throughout astrophysics. Yet again the notoriously hot solar corona is revealing unexpected results that may be important in astrophysics, from star formation to supernova remnants.

## ACKNOWLEDGMENTS

The author is grateful to Matthias Rempel for useful comments. Prof. J. Kuhn provided many comments and encouragement in the course of this work, without which this work would not have been completed. The referee provided excellent insightful comments which greatly helped the author in producing a far more readable paper. This material is based upon work supported by the National Center for Atmospheric Research, which is a major facility sponsored by the National Science Foundation under Cooperative Agreement No. 1852977.

## DATA AVAILABILITY STATEMENT

The exploratory research reported here uses IDL-based software developed by the first author without documentation. The “data” produced are exploratory in nature. Interested readers can request outputs from PGJ.

## REFERENCES

- Allen C. W., 1973, *Astrophysical Quantities*. Athlone Press, Univ. London
- Anderson L. S., Athay R. G., 1989, *Astrophys. J.*, 336, 1089
- Billings D. E., 1966, *A guide to the solar corona*. Academic Press, New York
- Bradshaw S. J., Cargill P. J., 2013, *ApJ*, 770, 12
- Braginskii S. I., 1965, *Reviews of Plasma Physics.*, 1, 205
- Brooks D. H., Warren H. P., 2016, *ApJ*, 820, 63
- Cally P. S., Robb T. D., 1991, *ApJ*, 372, 329
- Cargill P. J., De Moortel I., Kiddie G., 2016, *ApJ*, 823, 31
- Carlsson M., Stein R. F., 1995, *ApJ*, 440, L29
- Cheng C.-C., Doschek G. A., Feldman U., 1979, *ApJ*, 227, 1037
- Cowling T. G., 1956, *MNRAS*, 116, 114
- De Moortel I., Browning P., 2015, *Philosophical Transactions of the Royal Society of London Series A*, 373, 20140269
- Del Zanna G., Storey P. J., Badnell N. R., Andretta V., 2020, arXiv e-prints, p. arXiv:2006.08971
- Doschek G. A., Feldman U., 2000, *ApJ*, 529, 599
- Field G. B., 1965, *ApJ*, 142, 531
- Gilbert H. R., Hansteen V. H., Holzer T. E., 2002, *ApJ*, 577, 464

**Table 3.** List of modeled configurations and their outcomes.

Calc.	$L$ Mm	$P_W$ seconds	$\log_{10} F_W$ erg cm <sup>-2</sup> s <sup>-1</sup>	$\log_{10} T$ K	$\log_{10} n_p$ cm <sup>-3</sup>	$\log_{10} \frac{nH}{np}$	outcome
initial	20	...	...	6.24	8.82	-6.80	
1	10	1000	3	3.61	-0.97	2.99	EQ
2	10	1000	3+EUUV	4.08	8.29	-1.73	EQ
3	10	1000	4	3.61	-0.01	2.35	EQ
4	10	1000	4+EUUV	4.12	8.28	-1.76	EQ
5	10	1000	5	4.87	6.61	-3.97	EQ
6	10	1000	5+EUUV	4.51	8.13	-2.38	EQ
7	10	180	3	3.61	-0.91	2.96	EQ
8	10	180	3+EUUV	4.10	8.28	-1.74	EQ
9	10	180	4	4.52	6.00	-1.28	EQ
10	10	180	4+EUUV	4.30	8.23	-1.93	EQ
11	10	180	5	4.77	7.55	-4.00	EQ
12	10	180	5+EUUV	4.54	8.35	-3.01	EQ
13	20	1000	4	3.69			23800
14	20	1000	4+EUUV	4.19	6.44	-3.63	EQ
15	20	1000	5	4.86	6.25	-4.41	EQ
16	20	1000	5+EUUV	4.55	7.23	-3.43	EQ
17	20	180	3	3.67			20200
18	20	180	3+EUUV	4.15	6.04	-3.90	EQ
19	20	180	4	4.52	5.09	-1.59	EQ
20	20	180	4+EUUV	4.26	6.82	-3.33	EQ
21	20	180	5	4.68	7.09	-3.72	EQ
22	20	180	5+EUUV	4.55	7.52	-3.31	EQ
23	40	1000	4	3.94			36400
24	40	1000	4+EUUV	4.59	5.14	-5.26	EQ
25	40	1000	5	4.82	5.57	-4.30	EQ
26	40	1000	5+EUUV	4.62	5.80	-4.64	EQ
27	40	180	4	4.65	4.68	-3.78	EQ
28	40	180	4+EUUV	4.60	5.31	-5.09	EQ
29	40	180	5	4.67	5.98	-3.68	EQ
30	40	180	5+EUUV	4.60	6.03	-4.41	EQ
31	20	1000	4 g/2	4.62	6.26	-3.13	EQ
32	10	180	4 c	3.61	-1.33	3.12	EQ
33	10	180	5 c	4.77	7.55	-4.00	EQ

The calculations listed all begin with a near-equilibrium coronal model (the model for  $L = 20$  Mm is listed first). “+EUUV” indicates that EUV photo-ionization of H and He was included. Calculation 31 is identical to 13 except that half of the vertical solar gravity was used, assuming the bundle lies in a plane inclined at  $60^\circ$  to the local vertical. Calculations 32 and 33 were initiated from the final (very cool) solution of calculation 3. **The numbers in the last column refer to the time at which the calculation reached a collapsed state from which further calculations were not possible.**

- Gudiksen B. V., Carlsson M., Hansteen V. H., Hayek W., Leenaarts J., Martínez-Sykora J., 2011, *A&A*, 531, A154
- Habbal S. R., Ding A., Nassir M., Boe B., 2018, in AGU Fall Meeting Abstracts. pp SH43C–3710
- Hahn M., Savin D. W., 2014, *ApJ*, 795, 111
- Hansteen V., 1993, *ApJ*, 402, 741
- Hansteen V., et al., 2014, *Science*, 346, 1255757
- Hartmann L., MacGregor K. B., 1980, *ApJ*, 242, 260
- Holzer T. E., Flå T., Leer E., 1983, *ApJ*, 275, 808
- Hudson H. S., 1991, *Sol. Phys.*, 133, 357
- Hunter G., Kuriyan M., 1977, *Proceedings of the Royal Society of London Series A*, 353, 575
- Ionson J. A., 1978, *ApJ*, 226, 650
- Judge P., 2007, Technical Report NCAR/TN-473-STR, THE HAO SPECTRAL DIAGNOSTIC PACKAGE FOR EMITTED RADIATION (haos-diper) Reference Guide (Version 1.0). National Center for Atmospheric Research
- Judge P., Centeno R., 2008, *ApJ*, 687, 1388
- Judge P. G., de Pontieu B., McIntosh S. W., Olluri K., 2012, *ApJ*, 746, 158
- Klimchuk J. A., 2006, *Sol. Phys.*, 234, 41
- Kopp R. A., Poletto G., 1993, *ApJ*, 418, 496
- Korevaar P., van Leer B., 1988, *A&A*, 200, 153
- Kuhn J. R., Penn M. J., Mann I., 1996, *ApJ*, 456, L67
- Kuhn J. R., Arnaud J., Jaeggli S., Lin H., Moise E., 2007, *ApJ*, 667, L203
- Litwin C., Rosner R., 1993, *ApJ*, 412, 375
- Lyon J. G., Fedder J. A., Mobarry C. M., 2004, *Journal of Atmospheric and Solar-Terrestrial Physics*, 66, 1333
- Mann I., Kuhn J. R., 1998, *Advances in Space Research*, 21, 315
- Mariska J. T., 1987, *ApJ*, 319, 465
- Mariska J., 1992, The solar transition region. Cambridge astrophysics series Vol. 23, Cambridge University Press
- McClymont A. N., Canfield R. C., 1983, *ApJ*, 265, 483
- McIntosh S. W., de Pontieu B., Carlsson M., Hansteen V., Boerner P., Goossens M., 2011, *Nature*, 475, 477
- Moise E., Raymond J., Kuhn J. R., 2010, *ApJ*, 722, 1411
- Ofman L., Klimchuk J. A., Davila J. M., 1998, *ApJ*, 493, 474
- Ogawa H. S., Wu C. Y. R., Gangopadhyay P., Judge D. L., 1995, *J. Geophys. Res.*, 100, 3455
- Oran E. S., Mariska J. T., Boris J. P., 1982, *ApJ*, 254, 349
- Parker E. N., 1988, *ApJ*, 330, 474

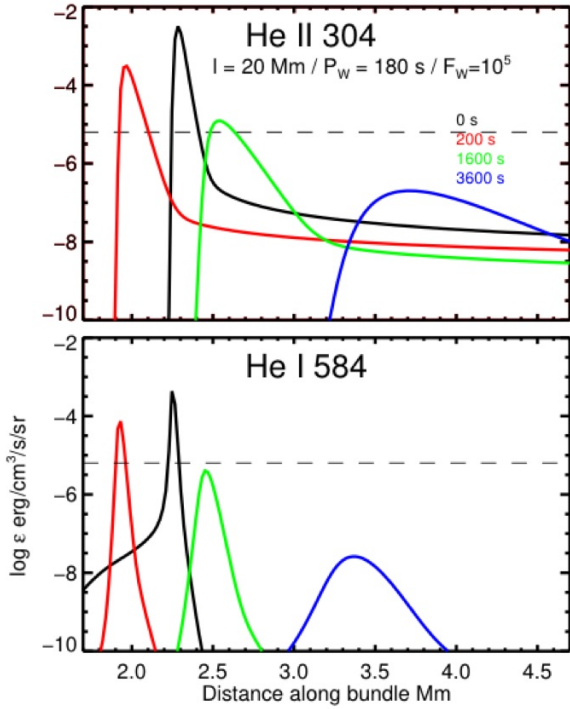


**Figure 8.** Emission coefficients for resonance lines of He and He<sup>+</sup> are shown as a function of position along the bundle, at four different times. The horizontal dashed line indicates the emission coefficient needed to contribute 10% of observed intensities, assuming a bundle thickness (cross-bundle path length for integration, equation 15) of 100 km.

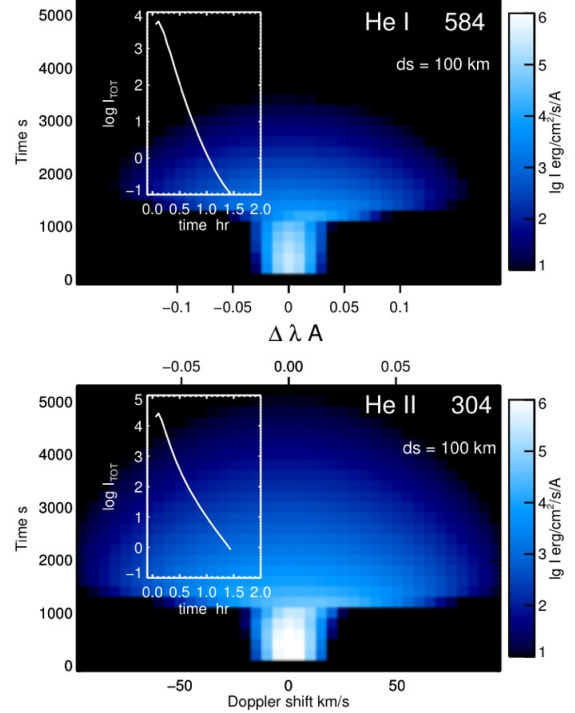


**Figure 9.** Evolution of the He and He<sup>+</sup> resonance line profiles and integrated intensities (inset plots). Units are  $\text{erg cm}^{-2} \text{s}^{-1} \text{sr}^{-1} \text{Å}^{-1}$  (images) and  $\text{erg cm}^{-2} \text{s}^{-1} \text{sr}^{-1}$  (line plots). The profiles shown were computed by identifying the brightest features along the bundle, and stacking these up to form a plot in time. This is what an instrument with a modest angular resolution of  $\geq 1$  Mm would observe. Data are shown for the footpoint near  $x = 0$  from calculation 22 of Table 3. The path length for integration (equation 15) was 100 km.

Parker E. N., 1991, *ApJ*, 376, 355

Parker E. N., 1994, *Spontaneous Current Sheets in Magnetic Fields with Application to Stellar X-Rays*. International Series on Astronomy and Astrophysics, Oxford University Press, Oxford

Parnell C. E., De Moortel I., 2012, *Philosophical Transactions of the Royal Society of London Series A*, 370, 3217

Peres G., Serio S., 1984, *Mem. Soc. Astron. Italiana*, 55, 749

Peter H., 2000, *A&A*, 360, 761

Peter H., 2006, *A&A*, 449, 759

Pietarila A., Judge P. G., 2004, *ApJ*, 606, 1239

Polito V., Testa P., Allred J., De Pontieu B., Carlsson M., Pereira T. M. D., Gošić M., Reale F., 2018, *ApJ*, 856, 178

Rempel M., 2017, *ApJ*, 834, 10

Roussev I., Galsgaard K., Judge P. G., 2002, *A&A*, 382, 639

Schmitt J. H. M. M., 1997, *aa*, 318, 215

Sokół J. M., Bzowski M., 2014, arXiv e-prints, p. arXiv:1411.4826

Spruit H. C., 2011, in Miralles, M. P. & Sánchez Almeida, J. ed., *The Sun, the Solar Wind, and the Heliosphere*. IAGA Special Sopron Book Series, Vol. 4. Berlin: Springer, p. 39

Tomczyk S., McIntosh S. W., Keil S. L., Judge P. G., Schad T., Seeley D. H., Edmondson J., 2007, *Science*, 317, 1192

Tóth G., Odstrčil D., 1996, *Journal of Computational Physics*, 128, 82

Williams T., et al., 2020, *ApJ*, 892, 134

Wójcik D., Kuźma B., Murawski K., Musielak Z. E., 2020, *A&A*,

635, A28

Wood B. E., Linsky J. L., Ayres T. R., 1997, *ApJ*, 478, 745

Zaitsev V. V., Shibasaki K., 2005, *Astronomy Reports*, 49, 1009